The Gulf Journal of Oncology

Indexed By PubMed and Medline Database

Issue 37, Sep 2021
ISSN No. 2078-2101

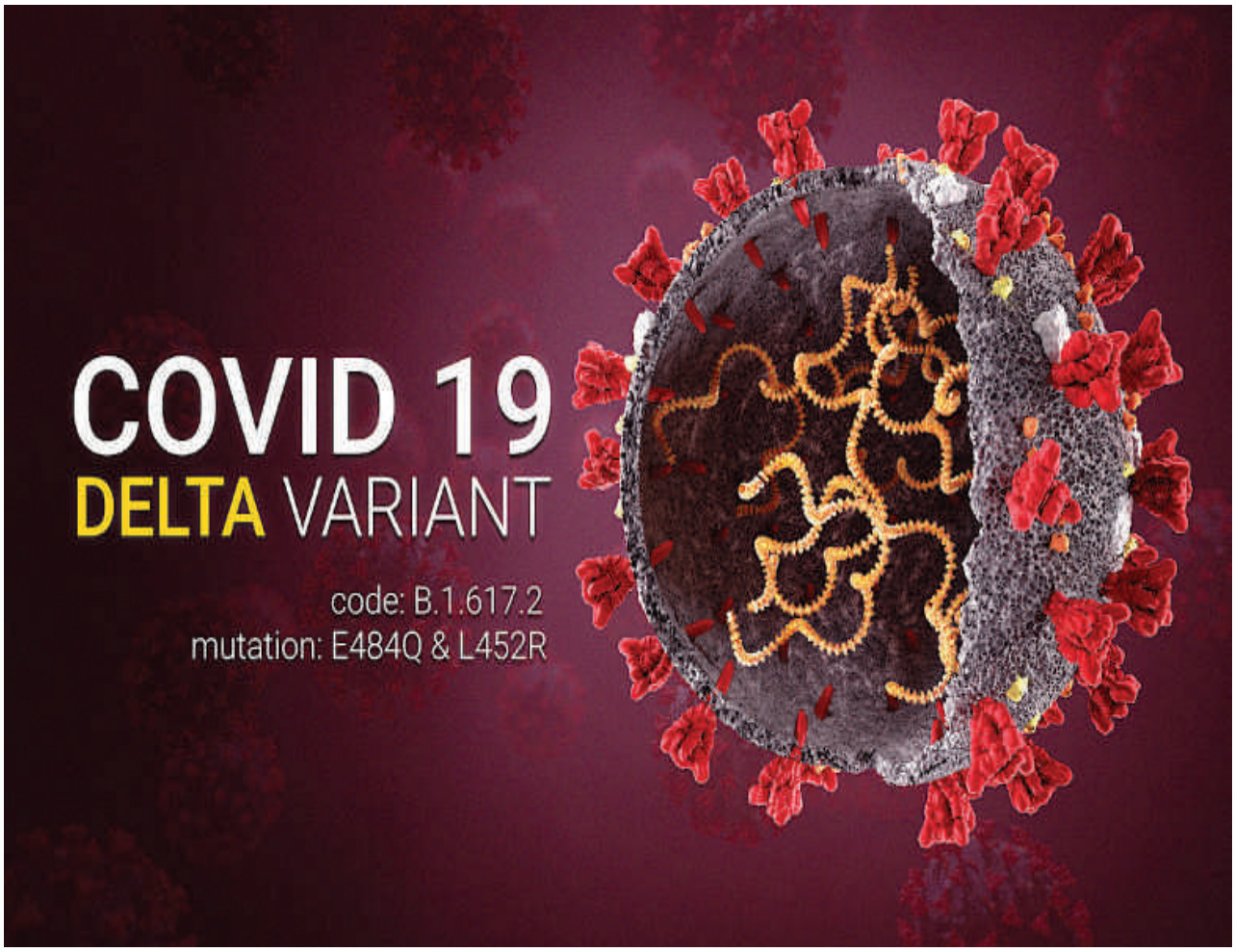

The Official Journal of the Gulf Federation For Cancer Control

Table of Contents

Original Articles

Review Article

Case Reports

Conference Highlights/Scientific Contributions

Original Article

Mutation Profiling of Intracranial Myxopapillary Ependymoma by Next Generation DNA Sequencing

Mohiuddin M. Taher [1,2,3], Abdulaziz Abdulnasser Alhussini[3], Muhammad Saeed[4], Mohammad Athar[1,2,3], Najwa Abdalkabeer A. Bantan[4], Raid A. Jastania[5,6], Kamal Bakour Balkhoyour[7], and Tahani H. Nageeti[8]

[1] Science and Technology Unit, Umm–al–Qura University, Makkah 21955, Saudi Arabia.
[2] Deanship of Scientific Research, Umm–Al–Qura University, Makkah 21955;
[3] Department of Medical Genetics, Faculty of Medicine, Umm–Al–Qura University, Makkah 21955, Saudi Arabia;
[4] Department of Radiology, Al–Noor Specialist Hospital, Makkah 24242, Saudi Arabia.
[5] Department of Pathology, College of Medicine, Umm–Al–Qura University, Makkah 24381;
[6] Department of Pathology, College of Medicine, King Abdul Aziz Medical City, Jeddah 21423:
[7] Department of Neurosurgery, Al–Noor Specialist Hospital, Makkah 24242, Saudi Arabia.
[8] Radiation Oncology Department, King Abdullah Medical City, Makkah 24246, Saudi Arabia;

Abstract

Objectives: Primary intracranial myxopapillary ependymomas (MPE) are very rare. In order to determine genomic changes in an intracranial MPE, we analyzed its mutation patterns by next generation DNA sequencing.

Methods: Tumor DNA was sequenced using an Ion PI v3 chip on Ion Proton instrument and the data were analyzed by Ion Reporter 5.6.

Results: In this tumor, NGS generated 6,298, 354 mapped reads using the Ion PI v3 Chip. The average reads per amplicon was 29,365, 100% of amplicons had at least 500 reads and the amplicons read end–to–end were 97.58%. In this tumor, NGS data analysis identified 12 variants, of which two were missense mutations, seven were synonymous mutations and three were intronic variants. Missense mutation in c.395G>A; in exon 4 of the IDH1 gene, and a missense mutation in c.215C>G; in exon 4 of the TP53 gene were found in this tumor were previously reported. The known synonymous mutations were found in this tumor were, in exon 14 of FGFR3 in c.1953G>A; in exon 12 of PDGFRA in c.1701A>G; in exon 18 of PDGFRA c.2472C>T; in exon 20 of EGFR in c.2361G>A; in exon 13 of RET in c.2307G>T; in exon 16 of APC in c.4479G>A; and in exon 2 of MET in c.534C>T. Additionally, a known intronic variant was identified in KDR and a known acceptor site splice variant in FLT3 (rs2491231) and a SNP in the 3'–UTR of the CSF1R gene (rs2066934) were also identified. Except, the frequency of IDH1 variant, the frequencies of other variants were high, and the p–values were significant and Phred scores were high for all of these mutations.

Conclusions: The variants reported in this tumor have not been detected in myxopapillary grade I ependymoma tumor by NGS analysis previously and we therefore report these variants in this case for the first time.

Keywords: Intracranial ependymoma, Myxoid degeneration, Myxopapillary ependymoma, Palisading necrosis, Ion Proton, Next Generation DNA sequencing, pediatric brain tumors.

Introduction

Ependymomas are brain tumors that develop in spinal cord, supratentorial areas, and the posterior fossa of the central nervous system, and they account for 2% of all intracranial tumors in adults, and almost 2% of all childhood cancers, and 10% of all malignant brain tumors in children.(1) The actual cause of ependymomas is unknown, however, ependymoma tumors differs in terms of tumor location, patient age, histological grade, and clinical behavior, and presents further challenges in understanding the development and progression of this disease. Many adult cases, occur in the spinal cord, on the

Corresponding Author: Dr Mohiuddin M. Taher, Deanship of Scientific Research, Umm–Al–Qura University, Al–Abidiya Campus, Taif Road, Makkah 24381, Saudi Arabia, TMMohiuddin@uqu.edu.sa; Taher23223@yahoo.com

other hand more than 90% of the pediatric ependymomas are intracranial, and majority of them arise in the posterior fossa. [2] As compared to younger children, the prognosis is better in older children, after five years event–free survival is less than 50% in intracranial pediatric ependymomas cases. For grade I, ependymomas the five–year overall survival rate is 92% and for anaplastic ependymoma it is 73%. [3]

World Health Organization (WHO) classification of ependymomas divide these tumors into 4 types: (A) grade I sub ependymomas, (B) grade I myxopapillary ependymomas, (C) grade II ependymomas, (D) grade II or III RELA fusion–positive ependymomas and grade III anaplastic ependymomas. [4] WHO grade I tumors, such as sub ependymomas and myxopapillary type tumors are usually benign, and typically slow growing, may hardly ever exhibit anaplastic features, however, exceptional cases of spinal myxopapillary ependymomas (MPE) with anaplastic features were also reported. [1–4] Myxopapillary ependymomas were first described by Kernohan in 1931. This tumor is distinguished by a papillary form of cuboidal cells around a vascular stromal core that undergoes mucinous degeneration. MPE occur almost in the lower part of the spinal column *viz.*, in conus medullaris, cauda equina, and filum terminale of the spinal cord with a peak incidence in the 4th decade of life, and they account for 27% of ependymomas occurring in the spinal cord. [5] However, atypical occurrences of MPEs in the cervico–thoracic spinal cord, lateral ventricle, brain parenchyma, and extradural regions were also known. [6] This tumor prevalence is 0.05 – 0.08 per 100,000 persons per year, however, 8% – 20% of all MPEs appear in the pediatric population and the overall survival at 5years was 97% for MPE. [5]

Gene expression studies have been reported in differentiating between intracranial and extra cranial ependymomas, but they are not clinically significant in directing therapy. [7] Comparative genomic hybridization (CGH) arrays data differentiates intracranial ependymomas from spinal ependymomas, and cDNA micro–arrays data of gene expression in ependymomas correlate with tumor location, tumor grade and the patient age. [8] Chromosomal abnormalities are relatively common in ependymomas, and chromosome 22q loss (LOH) has been the familiar abnormality found in ependymoma and, in some other tumors, gain of 1q or loss of 6q was observed. [9] Ebert *et al* have reported that the LOH on chromosome 22q in grade II and grade III spinal ependymomas, but it is not present in intracranial and myxopapillary ependymomas. [10] Previous report using next generation DNA sequencing (NGS) of a grade II ependymoma demonstrated copy number gain in MET and ATRX genes. [11] Overexpression of L1 cell adhesion molecule (L1CAM), and a homozygous deletion in CDKN2A was also reported in some aggressive supratentorial ependymomas. [12] Abedalthagafi *et al.*, have found reduced or absent of FOXJ1 expression and it is associated with poor survival rate using expression arrays, immunohistochemistry, and *in–situ* hybridization in anaplastic ependymomas, comparing to grade II, myxopapillary ependymoma from the lumbar spinal cord, cellular ependymoma and sub ependymoma. [13]

Ependymoma, like other cancers, is a genetic disease, however, the information regarding the mutational signatures by DNA sequencing is not very clearly useful clinically for classification of tumors and developing therapy, as compared to other cancers and brain tumors. Intracranial ependymomas differ from spinal ependymomas in the drug resistance, DNA repair enzymes expression, and these proteins expression is also dependent on the grade of ependymoma, however, very few mutations and gene amplifications were reported in this study. [14] Ebert *et al*, have found no NF2 mutations in intracranial and myxopapillary ependymomas, however, they have reported NF2 mutations in grade II spinal ependymomas. [10] In previously published reports, profiling of mutations by NGS method was carried out for one case of grade II ependymoma and in another case of grade III anaplastic ependymoma and in 8 intracranial ependymomas and 8 spinal cord ependymomas. [11, 15, 16] However, very few clinically significant mutations were reported in those studies. [11, 15, 16]. There are limited studies with intracranial and spinal myxopapillary ependymomas describing mutation profiling by NGS methods. In order to determine the mutation profile of MPE grade–I, we have sequenced DNA by NGS method from this tumor on Ion Proton system. These data provided an evaluation of mutational signatures of this grade–I ependymoma.

Methods

Ethical statement:

This study was performed in accordance with the principles of the Declaration of Helsinki. This study was approved by the Institutional Review Board (IRB) bioethics committee of King Abdullah Medical City (KAMC), Makkah, Kingdom of Saudi Arabia (IRB number 14–140). A written informed consent was obtained from the parents of this patient before starting the study.

Clinical specimen:

The three years old Saudi patient had undergone a tumor excision done by occipital craniotomy. The tumor was classified based upon similarity to the constituent cells of the central nervous system, such as astrocytes, oligodendrocytes and ependymal, glial cells, mitosis and

cell cycle–specific antigens, used as markers to evaluate proliferation activity and biological behavior according to the WHO grading system. [4] The final diagnosis was made following radiological, histopathological and immunological examinations. The tumor tissue (FFPE sections) used in this NGS analysis was obtained from the histopathology laboratory of Al–Noor Specialty Hospital Makkah.

Radiology and histopathological analysis:

A CT scan of the brain was performed by a multi–slice CT (MSCT), using a 64–detector–row scanner. Images were acquired with 5mm slice thickness throughout on a GE Medical Systems, light speed VCT, 64–slice multidetector CT (MDCT). Multi–sequential multi–planar pre and post Gadolinium MRI examination of the brain was performed on Siemens 3T MAGNETOM Skyra MRI scanner. High quality images were processed at low dose performance on Volara™ digital DAS (Data Acquisition System).

The excised tumor was fixed in 4% buffered formaldehyde, routinely processed and paraffin embedded. Four–micrometer–thick sections were prepared and routinely stained using with hematoxylin and eosin (H and E) on a Dako Coverstainer (Agilent). For immunohistochemistry, sections were collected on Citoglas adhesion microscope slides (Citotest). Antibodies used for immunohistochemistry were, mouse monoclonal vimentin (vim 3B4) (Ventana–Roche, Cat. No. 760–2512), anti–S100 (4C4.9) monoclonal (Cat.No790–2914), mouse monoclonal beta–catenin (Sigma–Aldrich, Cat. No. 224M–1), mouse monoclonal epithelial membrane antigen (EMA; E29) (Sigma–Aldrich, Cat. No. 247M–9), glial fibrillary acid protein (GFAP; EP672Y rabbit monoclonal; Ventana–Roche, Cat. No. 760–4345) and mouse monoclonal anti–Ki–67 (Leica Biosystems, Cat. No. KI67–MM1–L–CE). Immunohistochemistry was performed with the Ventana BenchMark XT automated Stainer (Ventana, Tucson, AZ). Following staining, images were acquired using NIKON Digital Microscope Camera – DS–Ri1, with image software NIS Elements v.4.0. Appropriate positive controls for all of the studied antibodies were used.

DNA isolation and NGS analysis:

DNA isolation was carried out using the QIAamp DNA Formalin–Fixed Paraffin–Embedded (FFPE) Kit (Cat. No. 56404, Qiagen). 5–10 FFPE sections of 5 microns were deparaffinized using xylene and ethanol, then the pellet was dried at 65 °C for 5 mins. The pellets were resuspended in ATL buffer to treat with proteinase K. The remaining steps were carried out according to the user manuals. DNA concentration was measured using Nanodrop2000C and 10 ng of DNA was used for NGS analysis. DNA was sequenced using the Ion PI v3 Chip Kit (Cat No. A25771) with the Ion Proton System from Thermo Fisher Scientific, USA. [15, 17] Libraries were prepared using Ion AmpliSeq cancer HotSpot Panel v1 (Cat No. 4471262) primer pools, and tagged with Ion Express Barcode Adapters 1–16 (Cat. No. 4471250). The Ion AmpliSeq Library Kit 2.0 (Cat No. 4475345), and Ion PI Hi–Q OT2 200 Kit (Cat No. A26434) was used for library and template preparation respectively. Sequencing was carried out using Ion PI Hi–Q Sequencing 200 Kit (Cat No. A26433) reagents and After sequencing, amplicon sequences were aligned to the human reference genome GRCh37 (hg19) in the target region of the cancer hotspot panel using the Torrent Suite Software v.5.0.2 (Thermo Fisher Scientific, USA). Variant call format files (vcf files) were generated by running the Torrent Variant Caller Plugin v5.2. The vcf file data were analyzed using Ion Reporter v5.6 (ThermoFisher Scientific, USA), which calculated allele coverage, allele frequency, allele ratio, variant impact, clinical significance, PolyPhen 2 scores, Phred scored, SIFT scores, Grantham scores and FATHMM scores. We have considered true mutations to be those with a Phred score above 20 and significant mutations called by Ion Reporter software were those with a p–value below 0.05. This vcf file analysis was also carried out by Advaita Bioinformatics' iVariantGuide.

Results

Clinical presentation and radiology:

A Saudi 3–year–old female patient, with a history of decreased oral intake, vomiting, fever, headaches, and weight loss was admitted into the neurosurgery unit. Examination of CT revealed a space occupying lesion (SOL), the patient subsequently underwent craniotomy. Brain CT (Figure 1 A and B) without contrast showed, a midline posterior fossa relatively hypo–dense soft tissue mass, likely seen within the fourth ventricle with subsequent dilatation of the supratentorial ventricular system. No intra or extra–axial area of recent blood density was noted. Intraventricular mass seen by CT examination in the fourth ventricle suggestive of ependymoma. MRI showed (Figure 1 C and D), a large well–defined mass is in the fourth ventricle dilating it. The mass is seen extending through to foramen of Magendi and extending to the right cerebellopontine angle (CPA). The tumor is causing indentation upon the brain stem posteriorly and from the left side. The mass shows iso– to hypo–intense on T1 WI and heterogeneously high SI on T2 WI with ring enhancement of the intraventricular portion and non–enhancing CPA extension. It measures about 2.5 x 4.5 x 3 cm (AP x TR x HT respectively).

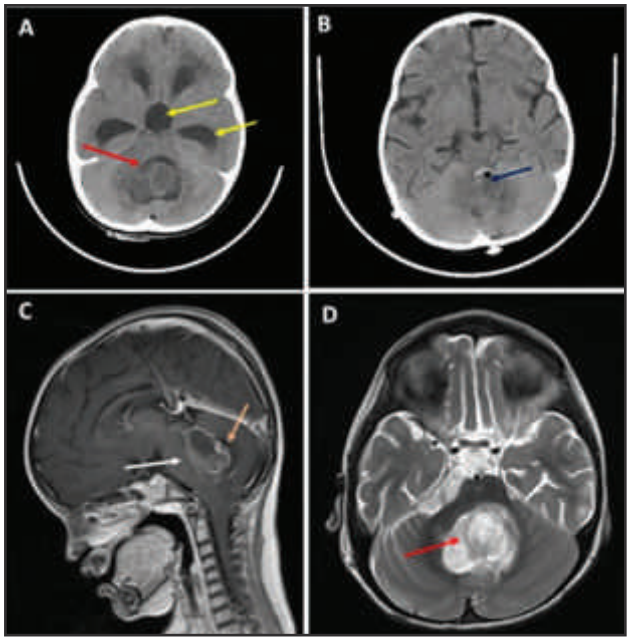

Figure 1: Pre–operative CT(A) showing Hypo–dense soft tissue mass (red) within the fourth ventricle with subsequent supratentorial hydrocephalic changes (yellow). Post– operative CT(B) do not show 4th ventricle mass lesion (Blue arrow) or hydrocephalic changes. Pre– operative MRI (C &D) showing a large well–Defined mass in the fourth ventricle. The mass is indenting the brain stem posteriorly (white) and display heterogeneous high SI on T2 WI (red) with post contrast ring enhancement (orange).

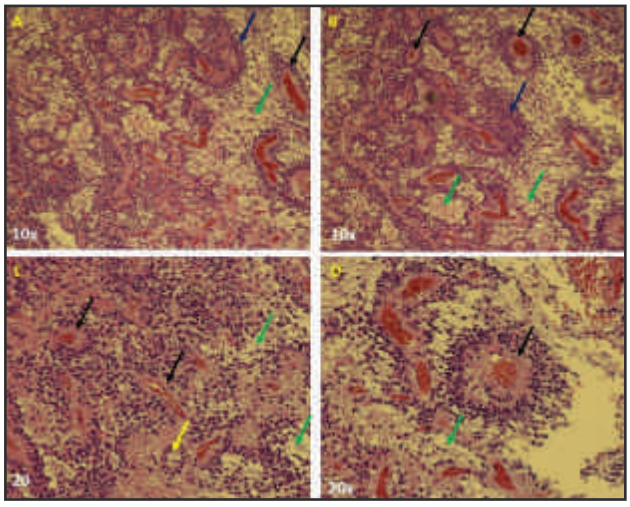

Figure 2: Hematoxylin and Eosin (H&E) staining of the myxopapillary ependymoma tumor: (A) Exhibiting cuboidal tumor cells (Blue arrow) which drape themselves about a basophilic mucinous material (Green arrow) that collars stromal blood vessels and collects in microcystic spaces, and pseudo–rosette (Black arrow). (B). Myxopapillary Ependymoma: Tumor cells (Blue arrow) showing pseudo–rosettes (Black arrows) and mucinous material (Green arrow) in rounded microcysts. (C) Few pseudo–rosettes (Black arrows) and occasional true ependymal rosette (Yellow arrows) containing a well–defined central lumen, admixed with mucinous material (Green arrows). (D) A prominent pseudo–rosette (Black arrow) with cytoplasmic processes of ependymal tumor cells condense around blood vessel. Mucinous material collected in microcysts (Green arrow).

Histopathology:

Microscopic examination showed the presence of ependymal cells evenly spaced perpendicular to a central lumen. Typical pattern composed of multiple papillary projections covered by cuboidal or short columnar ependymal cells. The ependymal cells are separated from the blood vessels by a zone of basophilic myxomatous material. The cells were epithelioid with only minimal nuclear variation and no mitotic activity. In terms of architecture, the tumor had microcystic areas with cuboidal cells arranged around pools of basophilic myxoid material. Perivascular pseudo rosettes predominate and are formed of ependymal cells arranged radially around fibrovascular cores with intervening myxoid material between the tumor cells and a central blood vessel. The vascular cores also contain focal hyalinization, however, there was no calcification or hemorrhage within the tumor found. Nuclear atypia, mitotic figures, and necrosis was absent. Histopathology of the tumors stained with Hematoxylin and Eosin (H&E) is shown Figures 2 and Figures 3. The MPE displayed cuboidal tumor cells which covers themselves about a basophilic mucinous material that collars stromal blood vessels and collects in microcystic spaces, and mucinous material in rounded microcysts (Figure 2 A and B). Figure 2 C, shows few pseudo–rosettes and occasional true ependymal rosette containing a well–defined central lumen, admixed with mucinous material. Also, a prominent pseudo–rosette with cytoplasmic processes of ependymal tumor cells condense around blood vessel, and mucinous material collected in microcysts are clear from Figure 2 D. In Figure 3A and B, prominent ependymal tumor cells and microcytic spaces containing mucinous material. Mucinous material separates draping tumor cells from a hyalinized vascular core and accumulates in rounded microcyst, no mitoses was seen (Figure 3 B). Immunostaining picture showed blood vessels within the mucoid material and demonstrated ependymoma cells stained strong diffusely with GFAP and vimentin (Figure 4 A and B), and S–100 stained strongly in cytosol (Figure 4 C), and beta–catenin stained membranous positive (Figure 4 D). However, EMA positivity showing punctate cytoplasmic (perinuclear dot–like positivity) staining fairly diagnostic of ependymal nature of the tumor cells was observed in this tumor (Figure 5A) and the immunostaining for Ki–67 was focally positive, with a proliferation of less than 3% (Figure 5 B). This myxoid ependymoma tumor stained negative with antibodies for P53, EGFR, neurofilament, E–cadherin, carcino embryonic antigen (CEA), chromogranin A, CK–7, Pan CK, and CK8/18 (not shown).

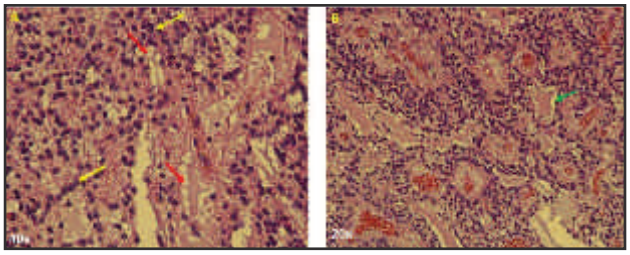

Figure 3: Hematoxylin and Eosin (H&E) staining showing myxopapillary ependymoma features. (A): showing prominent ependymal tumor cells (Yellow arrows) and microcystic spaces (Red arrows) containing mucinous material. (B) Mucinous material separates draping tumor cells from a hyalinized vascular core and accumulates in rounded microcyst (Green arrow).

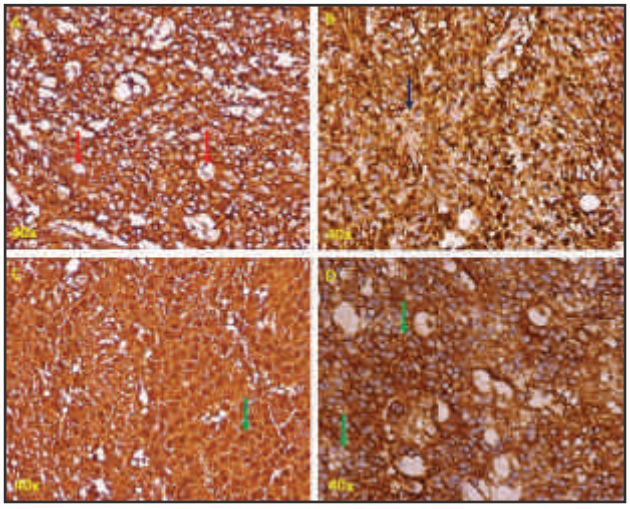

Figure 4: Immunostaining showing blood vessels (Red arrows) within the mucoid material (Blue arrow) and demonstrated ependymoma cells arranged in rosettes (Green arrow), with areas stained strong diffusely with GFAP and vimentin (A and B), and S–100 stained strongly in cytosol (C) and beta–catenin stained membranous positive (D).

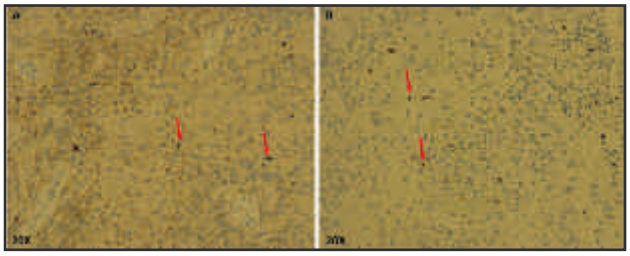

Figure 5: EMA positivity showing punctate cytoplasmic staining fairly diagnostic of ependymal nature of the tumor cells (A) and the immunostaining for Ki–67 was focally positive (B).

NGS data analysis variant identification and variant statistics:

Alignment to the target regions (CP.20131001. designed) of the reference genome (hg 19) was performed by the Ion Torrent Suite software v.5.0.2. For this tumor, NGS generated 6,298, 354 mapped reads using the Ion PI v3 Chip. Target base coverage analysis for the sequencing revealed 89.39% reads are on target, with 97.07% of uniformity of base coverage and the uniformity of amplicon coverage was 96.14%. The average target base coverage depth was 28,068. 100% of amplicons had at least 500 reads and the percentage of amplicons read end–to–end was 97.58%. Initial analysis by the Ion Reporter 5.6 program found that a total of 1625 variants passed all filters. Initial analysis by Advaita's iVariantGuide software showed 100% (1622) of variants passed all filters. The filter flags signify variants which do not meet certain criteria during variant calling. The distribution of these variants, based on chromosomal position, region within the gene, variant class, functional class, variant impact and clinical significance, are shown in doughnut charts A – F (Figure 6). As shown in doughnut chart A, chromosome 17 has the highest number of variants (26.5%) and chromosome 14 has lowest number of variants (0.2%). 98.5% of variants are exonic and, according to variant class distribution, 73.5% are SNPs, 69.9% are missense variants, 25.7% are high impact variants and 47.1% are pathogenic.

Summary of the all missense mutations found in grade I tumor is shown in Table 1. In this tumor NGS data analysis identified 12 variants out of which 2 are missense mutations, seven were synonymous mutations, and 3 were intronic variants. Known missense mutation (COSM28746) in exon 4 of the IDH1 gene, in c.395G>A; p. (Arg132His) and a known missense mutation in c.215C>G; p. (Pro72Arg) in exon 4 of the TP53 gene (rs1042522) were found in this tumor. We have shown for each target, frequency, allele coverage, allele ratio, p–value, and Phred score for these novel mutations in (Table 2). The p–value and Phred score were significantly high for all these mutations. As shown in Table 1, Seven synonymous mutations found in this tumor were, in exon 14 of FGFR3 in c.1953G>A; p. (Thr651Thr), exon 12 of PDGFRA in c.1701A>G; p.(Pro566Pro), in exon 18 of PDGFRA c.2472C>T; p. (Val824Val), exon 20 of EGFR in c.2361G>A; p.(Gln787Gln), exon 13 of RET in c.2307G>T; p.(Leu769Leu), exon 16 of APC in c.4479G>A; p.(Thr1493Thr) and in exon 2 of MET in c.534C>T; p. (Ser178Ser). These all synonymous variants were previously reported. Additionally, a known intronic variant was identified in KDR (c.798+54G>A), and a known splice site mutation (c.1310–3T>C) at an acceptor site in FLT3 (rs2491231) and a single nucleotide variant c.*1841TG>GA in the 3'–UTR of the CSF1R gene (rs2066934) were also identified. The frequencies of these missense mutations, were high, suggesting that these are germ line variants, whereas the IDH1 variant frequency was low (11.81%). However, FATHMM scores for the prediction of the functional consequences of a variant suggest that only the IDH1 variant is pathogenic, with a score of 0.94. As described in the COSMIC data

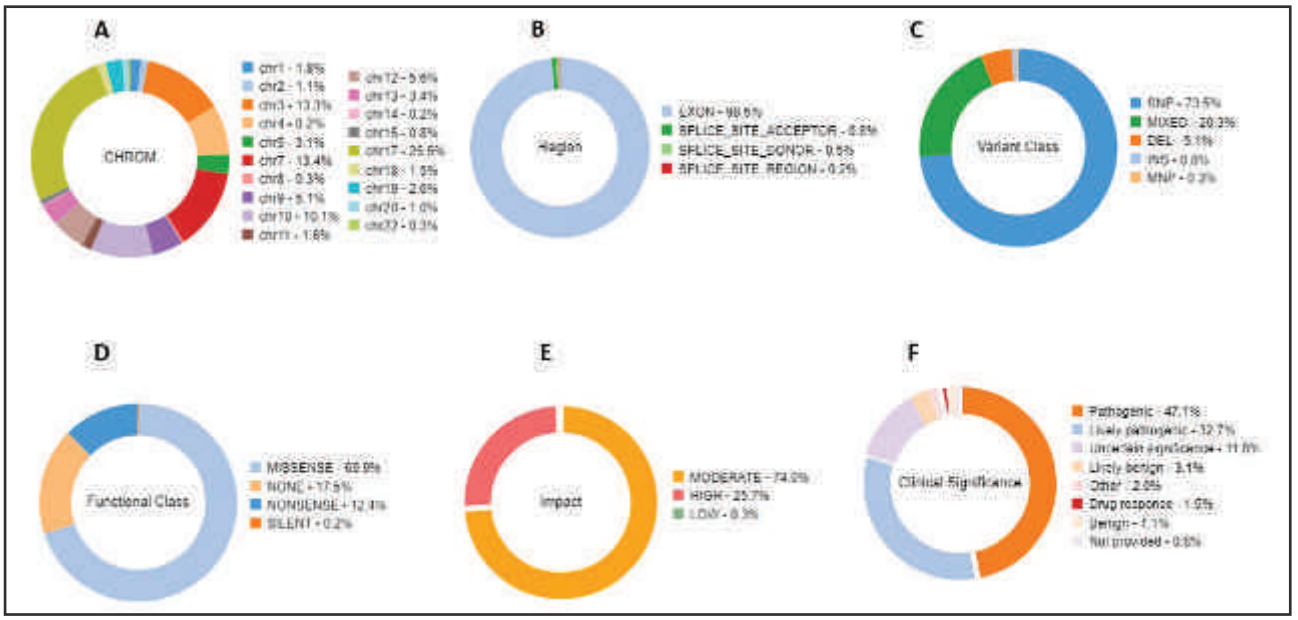

Figure 6: iVariant analysis of variant characteristics. Distribution of variants according to filters, showing characteristics including the relative number of variants located on each chromosome, variant class, substitution type and the functional consequences of each variant, in order to interpret and score the severity and impact of variants and therefore predict the severity of the disease. Doughnut charts in panels shows variants passed for each individual filter for (A) Chromosomal distribution, (B) Region in the gene, (C) Variant class, (D) Functional class (E) Variant impact on the protein function and (F) Clinical significance of the variants as annotated on the ClinVar database.

base, FATHMM scores above 0.5 are deleterious, but only scores ≥ 0.7 are classified as pathogenic. The coverage details of these synonymous mutations were described in (Table 2). Allele coverage, allele ratio, p–value, Phred quality score, sequencing coverage, alleles frequencies were also shown, the p–values and Phred quality score were significantly higher (Table 2).

Discussion

Nearly one–third of brain tumors in patients younger than three years old are ependymomas and constitute around 5%–9% of all neuroepithelial malignancies. [1–3] Most cases of intracranial MPEs are metastatic lesions with spinal origin, and primary intracranial MPE is an extremely rare tumor. Only 20 cases have been reported in the literature including ours, in the present case the tumor composed of perivascular pseudo rosettes with myxoid stroma and vascular cores. Microscopic examination of the tumor showed papillae with myxoid vascular cores lined by low columnar ependymal cells. In this case, a diagnosis was made based on the histopathological, immunohistochemical, radiologic findings and the location of the tumor confirming it as an MPE.

Most of the intracranial MPE tumors were reported to be positive for GFAP, S–100 and vimentin, and negative for cytokeratin, and chromogranin A and our results are in concordance with this observation. [18] The tumor cell in this case were stained strongly positive for GFAP, S–100, vimentin, and EMA staining revealed punctuated perinuclear dot–like structures a characteristic of ependymoma. There was no calcification or hemorrhage within the tumor, however a case of MPE with fine calcification was reported, and nuclear atypia, mitotic figures, and necrosis was absent in this case, also the Ki–67 index was low, these findings are in agreement with the published report. [19] In contrast to classical ependymoma, EMA positivity has been reported to be focal, or faint EMA staining, and in cases of intracranial MPE was negative also. [20] Immunohistochemical positivity for the p53 protein has not been previously described in primary intracranial MPEs, our results support this observation. [18] However, only one reported case of focal–positivity for the p53 protein, in a very low percentage (<1%) of the tumor cells, has been known in intracranial MPEs. [21] Changes in E–cadherin expression promote tumor invasion and metastasis. In spinal MPEs it has been reported that E–cadherin was negative. however, in another study with spinal MPE weak to moderate staining for E–cadherin was reported. [22, 23] In contrast with our present study, recently in a grade III anaplastic ependymoma tumor we have observed E–cadherin positivity. [15] In the present case EGFR stained negatively. EGFR in particular exhibits frequent gains and high–level amplifications in intracranial ependymomas, and its overexpression predicts poor patient outcome. [24]

Chromosomal Position	Ref	Observed Allele	% Frequency	Gene	Coding	AA Change	Phred Score	Exon
chr2:209113112	CG	TG	11.81	IDH1	c.395G>A	p. (Arg132His)	1293.83	4
chr4:1807894	G	A	100	FGFR3	c.1953G>A	p. (Thr651Thr)	31843.4	14
chr4:55141050	AGCCCAGA	AGCCCGGA	100.00	PDGFRA	c.1701A>G	p. (Pro566Pro)	35154.7	12
chr4:55152040	C	T	49.85	PDGFRA	c.2472C>T	p. (Va1824Val)	12256.3	18
chr4:55980239	C	T	100	KDR	c.798+54G>A	Intronic	30857	–
chr5:112175769	CGG	CAG	50.68	APC	c.4479G>A	p. (Thr1493Thr)	12379.6	16
chr5 :149433596	TG	GA	98.52	CSF1R	c.*1841TG>GA	3' UTR	30446.2	–
chr7:55249063	G	A	50.6	EGFR	c.2361G>A	p. (G1n787G1n)	10348.2	20
chr7:116339672	C	T	48.42	MET	c.534C>T	p. (Ser178Ser)	9640.32	2
chr10:43613843	G	T	56.88	RET	c.2307G>T	p. (Leu769Leu)	12386.2	13
chr13:28610183	A	G	50.85	FLT3	c.1310–3T>C	Splice acceptor region	10440.9	–
chr17:7579472	G	C	47.05	TP53	c.215C>G	p. (Pro72Arg)	11191.9	4

Table 1: Variants found in Grade–I Myxopapillary Ependymoma tumor by NGS

Genes	Coding	Allele Coverage	Allele Ratio	p–value	Coverage (x)	Variant ID
IDH1	c.395G>A	CG=1762, TG=236	CG=0.8819, TG=0.1181	0.00001	1998	COSM28746
FGFR3	c.1953G>A	G=0, A=1989	G=0.0, A=1.0	0.00001	1989	rs7688609
PDGFRA	c.1701A>G	AGCCCAGAT=0, AGCCCGGAT=1938	AGCCCAGAT=0.0, AGCCCGGAT=1.0	0.00001	1938	rs1873778
PDGFRA	c.2472C>T	C=1003, T=997	C=0.5015, T=0.4985	0.00001	2000	rs2228230
KDR	c.798+54G>A	C=0, T=1983	C=0.0, T=1.0	0.00001	1983	rs7692791
APC	c.4479G>A	CGG=973, CAG=1000	CGG=0.4932, CAG=0.5068	0.00001	1973	rs41115
CSF1R	c.*1841TG>GA	TG=29, GA=1936	TG=0.0148, GA=0.9852	0.00001	1965	rs2066934
EGFR	c.2361G>A	G=987, A=1011	G=0.494, A=0.506	0.00001	1998	rs1050171
MET	c.534C>T	C=1031, T=968	C=0.5158, T=0.4842	0.00001	1999	rs35775721
RET	c.2307G>T	G=858, T=1132	G=0.4312, T=0.5688	0.00001	1990	rs1800861
FLT3	c.1310–3T>C	A=983, G=1017	A=0.4915, G=0.5085	0.00001	2000	rs2491231
TP53	c.215C>G	G=1051, C=934	G=0.5295, C=0.4705	0.00001	1985	rs1042522

Table 2: Quality characteristics of Variants found in Grade–I ependymoma tumor

Despite several investigations, the correlation between histological grading of ependymoma tumors and their prognosis is unclear. Apart from histopathological grading, previous studies have focused on gross deletions and chromosomal abnormalities through cytogenetic studies and array–CGH profiling of ependymomas. [25] Mutation profiling of brain tumors by NGS methods is being utilized in clinical settings, like treatment, verifying resistance genes after treatment. [26] Ependymoma tumors profiling by NGS also reported recently, including MPE from spinal cord but for intracranial MPE mutation profiling has not been done. [11, 15, 16]

The IDH1 mutation c.395G>A; p. (Arg132His) detected in this grade I tumor was also recently reported in grade III anaplastic ependymoma, this substitution missense mutation has been reported previously (COSM28746) in glioma tumors also. [15] The frequencies of the IDH1 variant in the grade–I tumor was 11.81%, and in grade III tumor also it was low 4.81%. In this codon, a compound substitution c.394_395CG>GT (COSM28751) and another missense G>T mutation (COSM28750) are also known. Somatic IDH1 mutations in this codon have been found with greater frequency in diffuse astrocytoma's, oligodendrogliomas, oligoastrocytomas and secondary glioblastomas. However, several grade II and grade III ependymal tumors tested did not show this mutation. [27] For astrocytic tumors, the presence of this mutation is known to be associated with younger patients. [28] This observation supports our findings for this ependymoma tumor as the patient is three years–

old. This mutation is pathogenic, having a FATHMM score of 0.94. The SNP of Kinase insert domain receptor (KDR, rs7692791) was associated with poor overall survival (OS) among patients with gastric or biliary tract cancer who were treated with sunitinib. [29] Also, in the grade III tumor a missense mutation was observed in KDR gene in c.1416A>T; p. (Gln472His, rs1870377; COSM149673) in exon 11 previously. [15] But this missense mutation is not found in MPE in the present study. KRAS mutations were also found in the present study in c.43G>A (COSM538), in c.35G>T (COSM520), and in c.32C>T (COSM511) but the Phred score for these mutations were lower than 20, hence, we have not included these variants in the results.

In grade III tumor an intronic variant in PIK3CA (rs3729674) and one missense mutation of PIK3CA (COSM328028), a novel synonymous variant in FLT3 in c.1776T>C; p. (Val592Val), were reported by us recently, but in grade I tumor these variants were not found. [15] However, three intronic variants found in this study *viz*., in CSF1R gene (rs2066934), in FLT3 gene (rs2491231), in KDR gene (rs7692791) were also reported in grade–III ependymoma. The five synonymous mutations found in the present study *viz*., in PDGFRA (rs1873778), in FGFR3 (rs7688609) in RET (COSM4418405), in APC (COSM3760869) and in EGFR genes (rs1050171), were also detected in grade III ependymoma previously.[15] Additionally, two more synonymous mutation in *viz*., MET gene (rs35775721) PDGFRA gene (rs1873778) detected in the present study were not found in grade III tumor. [15] MET amplification and over expression is known in gliomas, and this was shown by NGS method also in a grade II ependymoma case. [11] The PDGFRA variant (rs1873778) and RET variant (COSM4418405) recently have been reported in a case of atypical choroid plexus papilloma also. [17]

Variants detected in this tumor, such as those in FGFR3, PDGFRA, CSF1R, EGFR, RET and FLT3 (c.1310–3T>C), were benign. All variants detected in this tumor have also been reported in other cancers: PDGFRA mutations in cervical adeno–squamous carcinomas; FGFR3 mutations in breast, endometrial and ovarian cancers; CSF1R mutations in prostate cancer; EGFR mutations in lung adenocarcinomas; RET mutations in thyroid carcinomas; However, these variants were not routinely found in brain tumors. Mutations in cancer driver genes such as PTEN, TP53, CDKN2A, and EGFR, which are frequently affected in gliomas, have been shown to be rare in ependymomas. In this tumor a TP53 mutation (c.215C>G, p. Pro72Arg, rs1042522) with a frequency of 47.94% was found. As reported by Zhang *et al*., this TP53 SNP rs1042522 allele G may be a potential protective factor against neuroblastoma in Chinese children. [30] Overall, in previous studies, a very low frequency of mutations was observed in both intracranial and spinal ependymomas and our findings also supports this observation. [11, 16, 26]

The Ion AmpliSeq Cancer HotSpot Panel consists of 50 oncogenes and tumor suppressor genes that are frequently mutated in several types of cancers. The detected mutations had high accuracy; 100% amplicons had at least 500 reads and 500x target base coverage was also 100%. This high level of accuracy and the high depth of coverage allows us to reliably detect low frequency mutations with high confidence. Allele coverage in most of the variants is around 2000x, the p–value was 0.00001 and the Phred score was very high for all the variants, indicating high confidence in the variants found in this tumor. Apart from its use in whole–exome sequencing, cancer panel analysis has also become common practice in NGS analysis. [11, 15, 16, 17] We have verified all mutations in various databases (COSMIC, ExAc and dbSNP) to confirm whether variants are novel in this MPE, however, all variants found in this study were known.

Conclusions: The variants reported in this tumor have not been detected in MPE grade I tumor by NGS analysis previously and we therefore report these variants in this case for the first time. This is the first NGS analysis report of the intracranial MPE tumor. We have identified 12 variants, of which two were missense mutations, seven synonymous mutations and three were intronic. The missense mutations were in IDH1 c.395G>A; and in TP53 c.215C>G respectively. The synonymous mutations were found in the present case are in FGFR3, PDGFRA, EGFR, RET, APC, and MET genes. Additionally, an intronic variants was identified in KDR and a splice site mutation at an acceptor site in FLT3 (rs2491231) and a single nucleotide variant in the 3'–UTR of the CSF1R gene (rs2066934) were also identified. The frequencies of the synonymous variants, were high, suggesting that these are germ line variants, and the frequencies of the missense were low suggesting these are somatic variants. The p–values were significant and Phred scores were high for all of these mutations. Further studies are warranted, with a greater number of tumors using NGS methods in MPE intracranial and also spinal ependymomas to identify the genetic signatures that may distinguish between these tumors.

Acknowledgements: We appreciate the technical help of Mrs. Rowa Abbas Bakhsh, Histopathology Division, Al–Noor Hospital, Makkah, and Mr. Mohammed Adil (Integrated Gulf Biosystems, Jeddah), for helping with Ion Proton. The authors would like to thank the staff of Science and Technology Unit at Umm Al–Qura University for the continuous support.

Grant Support: This study is Supported by National plan for Science, Technology and Innovation (MAARIFAH),

King Abdul Aziz City for Science and Technology, Award Number: 12–MED 2961–10, to MM. Taher.

Author roles: RAJ and KBB: Pathology and Surgery investigations; MMT and AAA: Data Curation and Writing the original draft; THN: Project Administration and Resources; MS and NAAB: Radiology investigation; MMT and MA: Methodology and Resources; MMT: Funding Acquisition, Supervision and Finalizing the manuscript.

Conflict of Interest: All authors agreed with the contents of this manuscript and all authors declare no conflicts of interest in publishing this manuscript.

References

1. Gerstner ER, Pajtler KW. Ependymoma. Semin Neurol. 2018;38(1):104–111.
2. Wu J, Armstrong TS, Gilbert MR. Biology and management of ependymomas. Neuro Oncol 2016;18: 902–913.
3. Vera–Bolanos E, Aldape K, Yuan Y, Wu J, Wani K, Necesito–Reyes MJ, Colman H, Dhall G, Lieberman FS, Metellus P, Mikkelsen T, Omuro A, Partap S, Prados M, Robins HI, Soffietti R, Wu J, Gilbert MR, Armstrong TS; CERN Foundation. Clinical course and progression–free survival of adult intracranial and spinal ependymoma patients. Neuro Oncol 2015; 17: 440–447.
4. Louis DN, Perry A, Reifenberger G, von Deimling A, Figarella–Branger D, Cavenee WK, Ohgaki H, Wiestler OD, Kleihues P, Ellison DW. The 2016 World Health Organization Classification of Tumors of the Central Nervous System: a summary. Acta Neuropathol. 2016; 131: 803–820.
5. Stephen JH, Sievert AJ, Madsen PJ, Judkins AR, Resnick AC, Storm PB, Rushing EJ, Santi M. Spinal cord ependymomas and myxopapillary ependymomas in the first 2 decades of life: a clinicopathological and immunohistochemical characterization of 19 cases. J Neurosurg Pediatr 2012;9 :646–653.
6. Frosch MP, Anthony DC, De Girolami U. Myxopapillary ependymoma. In: Kumar V, Abbas AK, Fausto N, (Ed) Robbins Pathologic Basis of Disease. 7. W B Saunders; 2005. pp. 1347–1419.
7. Witt H, Mack SC, Ryzhova M, Bender S, Sill M, Isserlin R, Benner A, Hielscher T, Milde T, Remke M, Jones DT, Northcott PA, Garzia L, Bertrand KC, Wittmann A, Yao Y, Roberts SS, Massimi L, Van Meter T, Weiss WA, Gupta N, Grajkowska W, Lach B, Cho YJ, von Deimling A, Kulozik AE, Witt O, Bader GD, Hawkins CE, Tabori U, Guha A, Rutka JT, Lichter P, Korshunov A, Taylor MD, Pfister SM. Delineation of two clinically and molecularly distinct subgroups of posterior fossa ependymoma. Cancer Cell. 2011; 20 :143–157.
8. Korshunov A, Neben K, Wrobel G, Tews B, Benner A, Hahn M, Golanov A, Lichter P. Gene Expression Patterns in Ependymomas Correlate with Tumor Location, Grade, and Patient Age. Am. J. Pathol 2003; 163: 1721–1727.
9. Mazewski C, Soukup S, Ballard E, Gotwals B, Lampkin B. Karyotype studies in 18 ependymomas with literature review of 107 cases. Cancer Genet Cytogenet 1999; 113 :1–8.
10. Ebert C, von Haken M, Meyer–Puttlitz B, Wiestler OD, Reifenberger G, Pietsch T and von Deimling A. Molecular genetic analysis of ependymal tumors. NF2 mutations and chromosome 22q loss occur preferentially in intramedullary spinal ependymomas. The American journal of pathology 1999; 155 :627–632.
11. Nikiforova MN, Wald AI, Melan MA, Roy S, Zhong S, Hamilton RL, Lieberman FS, Drappatz J, Amankulor NM, Pollack, Nikiforov YE, Horbinski C. Targeted next–generation sequencing panel (GlioSeq) provides comprehensive genetic pro□ling of central nervous system tumors. Neuro–Oncology 2016; 18: 379–387.
12. Matsumoto Y, Ichikawa T, Kurozumi K, Otani Y, Date I. Clinicopathological and Genetic Features of Supratentorial Cortical Ependymomas. World Neurosurg 2019 ;129: e417–e428.
13. Abedalthagafi MS, Wu MP, Merrill PH, Du Z, Woo T, Sheu SH, Hurwitz S, Ligon KL, Santagata S. Decreased FOXJ1 expression and its ciliogenesis programme in aggressive ependymoma and choroid plexus tumours. J Pathol 2016 ;238 :584–597.
14. Ferguson SD, Zhou S, Xiu J, Hashimoto Y, Sanai N, Kim L, Kesari S, de Groot J, Spetzler D, Heimberger AB. Ependymomas overexpress chemoresistance and DNA repair–related proteins. Oncotarget 2017; 9 : 7822–7831.
15. Butt M, Alyami S, Nageeti T, Saeed M, AlQuthami K, Bouazzaoui A, Athar M, Abduljaleel Z, Al–Allaf FA, Taher MM. Mutation profiling of anaplastic ependymoma grade III by Ion Proton by next generation DNA sequencing. [version 1; peer review: awaiting peer review] F1000Research 2019, 8 :613. https://doi.org/10.12688/f1000research.18721.1
16. Bettegowda C, Agrawal N, Jiao Y, Wang Y, Wood LD, Rodriguez FJ, Hruban RH, Gallia GL, Binder ZA, Riggins CJ, Salmasi V, Riggins GJ, Reitman ZJ, Rasheed A, Keir S, Shinjo S, Marie S, McLendon R, Jallo G, Vogelstein B, Bigner D, Yan H, Kinzler KW, Papadopoulos N. Exomic Sequencing of Four Rare Central Nervous System Tumor Types. Oncotarget 2013; 4: 572–583.
17. Taher MM, Hassan AA, Saeed M, Jastania RA, Nageeti TH, Alkhalidi H, Dairi G, Abduljaleel Z, Athar M, Bouazzaoui A, El–Bjeirami WM, Al–Allaf FA. Next generation DNA sequencing of atypical choroid plexus papilloma of brain: Identification of novel mutations in a female patient by Ion Proton. Oncol. Lett. 2019. DOI: 10.3892/ol.2019.10882.
18. Matyja E, Naganska E, Zabek M, Koziara H. Myxopapillary ependymoma of the lateral ventricle with local recurrences: histopathological and ultrastructural analysis of a case. Folia Neuropathol 2003; 41:51–57.
19. Lim SC, Jang SJ. Myxopaplillary ependymoma of the fourth ventricle. Clin Neurol Neurosur 2006: 108:211–214.

20. Schittenhelm J, Becker R, Capper D, Meyermann R, Iglesias–Rozas JR, Kaminsky J, Mittelbronn M. The clinicosurgico–pathological spectrum of myxopapillary ependymomas: report of four unusual cases and review of the literature. Clin Neuropathol 2008; 27:21–28.

21. Sparaco M, Morelli L, Piscioli I, Donato S, Catalucci A, Licci S. Primary myxopapillary ependymoma of the cerebellopontine angle: Report of a case. Neurosurg Rev 32:241–244.

22. Lamzabi I, Arvanitis LD, Reddy VB, Bitterman P, Gattuso P. Immunophenotype of myxopapillary ependymomas. Appl Immunohistochem Mol Morphol 2013 ;21:485–489.

23. Tena–Suck ML, Castillejos–Lopez M, Diaz–Alba A, Sanchez–Garibay C. Expression of glial acidic fibrillary protein delta and E–cadherin in ependymomas; clinic–pathological and immunohistochemistry correlation. J Histol Histopath 2015; 2: Article 17. doi: 10.7243/2055–091X–2–17.

24. Mendrzyk F, Korshunov A, Benner A, Toedt G, Pfister S, Radlwimmer B, Lichter P. Identification of gains on 1q and epidermal growth factor receptor overexpression as independent prognostic markers in intracranial ependymoma. Clin Cancer Res 2006:12(7 Pt 1):2070–2079.

25. Ward S, Harding B, Wilkins P, Harkness W, Hayward R, Darling JL, Thomas DG, Warr T. Gain of 1q and loss of 22 are the most common changes detected by comparative genomic hybridization in pediatric ependymoma. Genes Chrom Cancer 2001; 32 :59–66.

26. Miller CA, Dahiya S, Li T, Fulton RS, Smyth MD, Dunn GP, Rubin JB, Mardis ER. Resistance–promoting effects of ependymoma treatment revealed through genomic analysis of multiple recurrences in a single patient. Cold Spring Harb Mol Case Stud 2018; 4(2): pii: a002444.

27. Mellai M, Piazzi A, Caldera V, Monzeglio O, Cassoni P, Valente G, Schiffer D. IDH1 and IDH2 mutations, immunohistochemistry and associations in a series of brain tumors. J Neurooncol 105 :345–357.

28. Balss J, Meyer J, Mueller W, et al. Analysis of the IDH1 codon 132 mutation in brain tumors. Acta Neuropathol 2008; 116:597–602.

29. Maeng CH, Yi JH, Lee J, Hong JY, Choi MK, Jung HA, Park JO, Park SH, Park YS, Kang WK, Lim HY. Effects of single nucleotide polymorphisms on treatment outcomes and toxicity in patients treated with sunitinib. Anticancer Res 2013 ;33 :4619–4626.

30. Zhang J, Yang Y1, Li W, Yan L, Zhang D, He J, Wang J. TP53 gene rs1042522 allele G decreases neuroblastoma risk: a two–center case–control study. J Cancer 2019 ;10 :467–471.